VOL. 18, NO. 3, FEBRUARY 2023 ISSN 1819-6608
ARPN Journal of Engineering and Applied Sciences

www.arpnjournals.com

EFFECTS OF MAGNETO HYDRODYNAMIC AND SURFACE ROUGHNESS ON SQUEEZE FILM CHARACTERISTICS BETWEEN PARALLEL STEPPED PLATES WITH MICRO POLAR FLUID

M. Faizan Ahmed and E. Sujatha
Department of Mathematics, SRM Institute of Science and Technology, Kattankulathur, India
E-Mail: fm0834@srmist.edu.in

ABSTRACT

In this paper, the effects of surface roughness and magnetohydrodynamic (MHD) combined together with squeeze film characteristics of micropolar fluid on the parallel stepped plate are analyzed. On the basis of Christensen's theory, the one-dimensional structure of the radial and azimuthal roughness patterns is considered. The modified stochastic Reynold's equation is derived for these two types of roughness patterns by taking into account micropolar fluid. The analytical approximation solution for mean fluid film pressure and workload is obtained. The results are compared between the MHD and non-MHD cases. On the whole, it is observed that with an increase in roughness parameter, the pressure and workload increase with distance and height respectively.

Keywords: micropolar fluid, MHD, parallel stepped plates, squeeze film technique, surface roughness.

1. INTRODUCTION

The hydrodynamic squeeze film property has already drawn a lot of attention because of the wide range of industrial applications it has, including gyroscopes, rolling elements, mechanical components, power transmission equipment, damping films for aircraft engines, and skeletal joints in human bodies. Numerous fields of industrial engineering and applied science, including parts of the machine, components of an automobile, joints of animals, and wet-clutch plates, matching gears, demonstrate the importance of applications of squeeze-film technology. Most research on the properties of squeeze films focuses on the use of Newtonian lubricants as investigated by Hamarock[6], Hays[10], and many more. When additives are added to lubricants it alters their nature with respect to shear rate and this enables to increase in the workload of the bearing in which such a lubricant is employed. Eringen's [4] work in 1966 threw light on a new kind of fluid that had particles that were suspended and had an independent motion. This new fluid which he named micropolar, is a subclass of the microfluids [5], which have the properties of local inertial, inertial spin, and a couple of stress imported in them. Siddangouda [17] analyzed the micropolar fluid on parallel stepped plates and compared it with the Newtonian case and concluded that the micropolar fluid had improved workload. A porous media is defined by the presence of pores, which are frequently filled with fluid. A wide range of machineries on a daily basis employs porous bearings to support a rotating shaft. When it comes to noise, lubrication loss, early failure, and intermittent friction, these bearings are crucial. The fundamental framework of the physical-mathematical system, known as magnetohydrodynamics (MHD), studies the dynamics of magnetic fields in electrically conducting fluids. The fundamental idea behind MHD is that magnetic fields have the ability to change the strengths of geometry and magnetic field, induce currents in a flowing conductive fluid and produce fluid forces. Many researchers are motivated to study MHD because of the substantial industrial significance of MHD, including MHD pumps, MHD generators, etc. The study of MHD was taken up by many researchers like Kuzma[12], and Shukla[18] to name a few. Bujurke and Kudenatti [2], Lin [13], Brinda Halambi, Hanumagowda [1], and many more analyzed the effects of MHD on different types of geometries. Naduvinamani and S. Santosh [15] analyzed the MHD effects on finite journal bearing. Hanumagowda *et al* [7] had taken up the study of the influence of hydromagnetic on a parallel stepped-to plate and concluded that the effects of MHD enhance the workload compared to non-magnetic cases. Naduvinamani and Shridevi [16] had taken up the study on parallel plates with micropolar fluid and concluded that the applied magnetic field increases the pressure and workload.

Surface roughness is the fundamental part of fabrication and has drawn the attention of many researchers. Porosity and surface roughness have a strong interdependence among them. The order of mean separation amongst the layers which have been separated by the lubricant is most of the time same as that of the size of the wedges and the valleys created due to the surface roughness. This influences the way in which the bearing system performs. This kindled the interest of many researchers to study surface roughness either through deterministic models or stochastic models. Of these two models, the stochastic model, due to their practice and applicability is employed in studying the surface asperities of the bearings which can be assumed to be a random variable. Christenson and Tonder [3] proposed a new stochastic model based on these randomly distributed variables to investigate the roughness created on the surface of the bearing due to its continuous operation. There are several studies about surface roughness among the researchers like Halambi [8], Murmu and Rao [14], and S. kesavan *et al* [11] with micropolar fluid and MHD on different geometries. Siddangouda [19] studied the roughness effects in inclined stepped composite bearing, Hanumagowda *et al* [9] analyzed the roughness effects on curved annular plates and it was concluded that the azimuthal roughness pattern increases the pressure, workload, and squeeze film time compared to radial roughness. In the current article, the impact of the MHD and Â surface roughness on workload through parallel stepped plate lubrication with micro-polar fluid squeeze films has been analyzed. The micropolar fluid theory is used to derive the modified Reynolds equation. The influence of the surface roughness on pressure and workload is obtained.

2. GEOMETRY OF THE BEARING

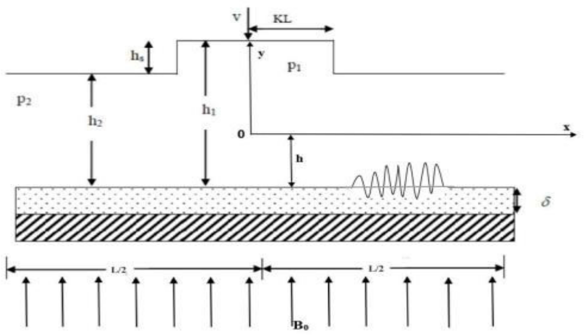

Figure-1. Parallel Stepped Plate.

The bearing system's design is depicted in the picture. Plate geometry is assumed to be parallel stepped plates. The upper plate, which has a central step with height, approaches the lower plate, which is flat and porous in nature in the direction of x, with a constant velocity $v = \partial(2h)/\partial t$. The region between the plates is filled with a micropolar fluid.

3. MATHEMATICAL FORMULATION

Considering the typical assumptions being made for a hydrodynamic lubrication applied to a layer, the following hold true for a micropolar fluid, as proposed by Eringen [4], subject to an applied magnetic field B_0.

$$\frac{\partial u}{\partial x} + \frac{\partial v}{\partial y} = 0 \tag{1}$$

$$\frac{\partial p}{\partial y} = 0 \tag{2}$$

$$\left(\mu + \frac{\chi}{2}\right)\frac{\partial^2 u}{\partial y^2} + \chi\frac{\partial v_2}{\partial y} - \sigma B_0^2 u - \frac{\partial p}{\partial x} = 0 \tag{3}$$

$$\gamma\frac{\partial^2 v_2}{\partial y^2} - 2\chi v_2 - \chi\frac{\partial u}{\partial y} = 0 \tag{4}$$

where equation (1),(3) and (4) represents the conservation of mass, conservation of linear momentum and conservation of angular momentum respectively. Variables (u, v) represent velocity components in the directions (x, y). v_2 is velocity component of Micro-rotation, p represents film pressure, σ denotes electrical conductivity of the fluid, γ denote viscosity co-efficient of micropolar fluid, χ denote spin viscosity, μ indicates Newtonian viscosity. B_0 denote magnetic field, let h be the thickness of film.

For the upper plate $(y = h)$ the boundary conditions (B.C) are

$$u = 0, v = \frac{\partial(2h)}{\partial t}, v_2 = 0 \tag{5}$$

And for the lower plate $(y = -h)$ it is given by

$$u = 0, v = v^\star, v_2 = 0 \tag{6}$$

where the $v^\star$ is the velocity component of Darcy.

By solving the equation (3) and (4) and using the boundary condition (5) and (6), the expression for u is obtained in the form

$$u = -\frac{\begin{matrix}\Phi_2 \sinh(g_2 h)\,[\cosh(g_1 h) - \cosh(g_1 y)] - \\ \Phi_1 \sinh(g_1 h)\,[\cosh(g_2 h) - \cosh(g_2 y)]\end{matrix}}{\sigma B_0^2\begin{bmatrix}\Phi_2 \sinh(g_2 h)\cosh(g_1 h) - \\ \Phi_1 \sinh(g_1 h)\cosh(g_2 h)\end{bmatrix}}\frac{\partial p}{\partial x}$$

where,

$$g_1 = \left(\frac{\alpha_1 + \sqrt{\alpha_1^2 - 4\beta_1}}{2}\right)^{\frac{1}{2}},$$

$$g_2 = \left(\frac{\alpha_1 - \sqrt{\alpha_1^2 - 4\beta_1}}{2}\right)^{1/2},$$

$$\alpha_1 = \frac{4\mu\chi + 2\gamma\sigma B_0^2}{\gamma(2\mu + \chi)},$$

$$\beta_1 = \frac{4\chi\sigma B_0^2}{\gamma(2\mu + \chi)}$$

$$\Phi_1 = \frac{2\sigma B_0^2 - (2\mu + \chi)g_1^2}{2\chi g_1},$$

$$\Phi_2 = \frac{2\sigma B_0^2 - (2\mu + \chi)g_2^2}{2\chi g_2}$$

Darcy's law prescribes the format for the flow of the fluid through porous matrix given by

$$\hat{q} = -\frac{k}{(\mu + \chi)}\nabla p^\star \tag{7}$$

where the vector $\hat{q} = (u^\star, v^\star)$ is the velocity component of Darcy. k and $p^\star$ represents the permeability and pressure of porous zone respectively. The equation (1) of lubricant in porous medium turn out to be

$$\frac{\partial^2 p^\star}{\partial x^2} + \frac{\partial^2 p^\star}{\partial y^2} = 0 \tag{8}$$

Then the component of velocity $v^\star$ at the lower surface $(y = -h)$ is,

ARPN Journal of Engineering and Applied Sciences

$$(v^{\star})_{y=-h} = \left(\frac{k\delta}{\mu+\chi}\right)\left(\frac{\partial^2 p}{\partial x^2}\right) \quad (9)$$

where δ is the thickness of the porous layer,

The mass conservation equation (4) on application of the B.C (5) and (6) leads to the modified Reynolds equation that takes the form

$$\frac{\partial^2 p}{\partial x^2}\left[G(h,N,L,M) + \frac{k\delta}{(\mu+\chi)}\right] = -12\frac{dh}{dt} \quad (10)$$

where $G(h,N,L,M) = \frac{(A_1-B_1)}{\sigma B_0^2 f_1 f_2 (A_2-B_2)}$

$$A_1 = f_2\Phi_2 sinh(f_2\text{h})$$
$$[cosh(f_1\text{h})f_1 - sinh(f_1\text{h})]$$

$$B_1 = f_1\Phi_1 sinh(f_1\text{h})$$
$$[cosh(f_2\text{h})f_2 - sinh(f_2)]$$

$$A_2 = \Phi_2 sinh(f_2\text{h})cosh(f_1\text{h})$$
$$B_2 = \Phi_1 sinh(f_1\text{h})cosh(f_2\text{h})$$

$$f_1 = \left(\frac{\alpha_1 + \sqrt{\alpha_1^2 - 4\beta_1}}{2}\right)^{1/2},$$
$$f_2 = \left(\frac{\alpha_1 - \sqrt{\alpha_1^2 - 4\beta_1}}{2}\right)^{1/2}$$

$$\alpha_1 = \frac{4\mu\chi + 2\gamma\sigma B_0^2}{\gamma(2\mu+\chi)},$$
$$\beta_1 = \frac{4\chi\sigma B_0^2}{\gamma(2\mu+\chi)}$$

$$\Phi_1 = \frac{2\sigma B_0^2 - (2\mu+\chi)f_1^2}{2\chi f_1},$$
$$\Phi_2 = \frac{2\sigma B_0^2 - (2\mu+\chi)f_2^2}{2\chi f_2}$$

Using the following dimensionless variables and quantities

$$x^{\star} = \frac{x}{A}, H^{\star} = \frac{h}{h_0} = \frac{2h}{H_0}, \alpha_1^{\star} = \alpha_1 H_0^2, \beta_1^{\star} = \beta_1 H_0^4,$$
$$g_1^{\star} = g_1 H_0, g_2^{\star} = g_2 H_0, \Phi_1^{\star} = \Phi_1 H_0,$$
$$\Phi_2^{\star} = \Phi_2 H_0, \Psi = \frac{k\delta}{H_0^3}$$

the dimensionless modified Reynolds equation takes the form

$$\frac{\partial^2 p}{\partial x^2}[G^{\star}(H^{\star},N,L^{\star},M,\Psi)] = -12 \quad (11)$$

The mathematical expression for film thickness $H_i = H_i + h_s(x,y,\xi)$ i=1,2 denotes the H_1 inlet hieght which also happens to be the maximum film thickness and H_2 outlet height which is also represents the minimum film thickness and takes the following form to represent surface roughness. $\xi$is the index parameter which determines exact roughness pattern. Let $f(h_s)$ be the probability function of the stochastic film thickness h_s. Taking the stochastic averaged of (11) with respect to $f(h_s)$ the averaged modified Reynolds equation is obtained in the form

$$\frac{\partial^2 p}{\partial x^2}[E(G^{\star}(H^{\star},N,L^{\star},M,\Psi))] = -12 \quad (12)$$

$$E(G^{\star}(H^{\star},N,L^{\star},M,\Psi)) = \frac{24(C_1 - D_1)}{\sigma B_0^2 g_1 g_2 (C_2 - D_2) + \left(12\Psi\left(\frac{1-N^2}{1+N^2}\right)\right)}$$

$$C_1 = \tilde{f}_2\Phi_2^{\star} sinh(0.5\tilde{f}_2 H^{\star})$$
$$[cosh(0.5\tilde{f}_1 H^{\star})0.5\tilde{f}_1 H^{\star} - sinh(0.5\tilde{f}_1 H^{\star})]$$

$$D_1 = \tilde{f}_1\Phi_1^{\star} sinh(0.5\tilde{f}_1 H^{\star})$$
$$[cosh(0.5\tilde{f}_2 H^{\star})0.5\tilde{f}_2 H^{\star} - sinh(0.5\tilde{f}_2 H^{\star})]$$

$$C_2 = \Phi_2^{\star} sinh(0.5\tilde{f}_2 H^{\star})cosh(0.5\tilde{f}_1 H^{\star})$$
$$D_2 = \Phi_1^{\star} sinh(0.5\tilde{f}_1 H^{\star})cosh(0.5\tilde{f}_2 H^{\star})$$

$$\tilde{f}_1 = f_1 H_0 = \left(\frac{\alpha_1^{\star} + \sqrt{\alpha^{\star 2}_1 - 4\beta_1^{\star}}}{2}\right)^{1/2},$$

$$\tilde{f}_2 = f_2 H_0 = \left(\frac{\alpha_1^{\star} - \sqrt{\alpha^{\star 2}_1 - 4\beta_1^{\star}}}{2}\right)^{1/2}$$

$$\beta_1^{\star} = \beta_1 H_0^2 = \frac{N^2 M^2}{L^2},$$
$$\Phi_1^{\star} = \Phi_1 H_0 = \frac{M^2(1-N^2) - \widetilde{f_1^2}}{2N^2\widetilde{f_1^2}},$$
$$\Phi_2^{\star} = \Phi_2 H_0 = \frac{M^2(1-N^2) - \widetilde{f_2^2}}{2N^2\widetilde{f_2^2}},$$
$$N = \left(\frac{\chi}{2\mu+\chi}\right)^{\frac{1}{2}}, L^{\star} = \frac{\left(\frac{\chi}{4\mu}\right)^{\frac{1}{2}}}{H_0},$$
$$M = B_0 H_0\left(\frac{\sigma}{\mu}\right)^{\frac{1}{2}}$$

where expectancy operator $E(\star)$ is given by

$$E(\star) = \int_{-\infty}^{\infty} f(h_s)ds \quad (13)$$

$$f(h_s) = \begin{cases} \frac{35}{32c^7}(c^2 - h_s^2)^3 & -c < h_s < c \\ 0 & Otherwise \end{cases}$$

In general, there are two types of roughness pattern - radial and azimuthal, that is assumed to be in x and y direction. In this paper the roughness structure is assumed to be one dimensional radial roughness. While

ARPN Journal of Engineering and Applied Sciences

rotating the co-ordinates axes the radial and azimuthal roughness becomes identical.

$$\frac{\partial^2 E(p)}{\partial x^2}[E(G^\star(H^\star,N,L^\star,M,\Psi))] = -12 \tag{14}$$

$$\frac{\partial^2 E(p)}{\partial x^2}\left[\frac{1}{E(G^\star(H^\star,N,L^\star,M,\Psi))}\right] = -12 \tag{15}$$

Combining the above equations

$$\frac{\partial^2 E(p)}{\partial x^2}[Q(H^\star,N,L^\star,M,\Psi,c^\star)] = -12 \tag{16}$$

where

$$Q(H^\star,N,L^\star,M,\Psi,c^\star) = \begin{cases} E[G(H^\star,N,L^\star,M,\Psi)] \\ (Radial\ \ roughness) \\ E\left[\dfrac{1}{G(H^\star,N,L^\star,M,\Psi)}\right]^{-1} \\ (Azimuthal\ \ roughness) \end{cases}$$

where

$$Q(H^\star,N,L^\star,M,\Psi,c^\star) = \tag{17}$$

$$\frac{24(a_1-b_1)}{\sigma B_0^2 s_1^\star s_2^\star (a_2-b_2) + \left(12\Psi\left(\frac{1-N^2}{1+N^2}\right)\right)}$$

$$a_1 = s_2^\star \xi_2^\star sinh(0.5 s_2^\star H^\star)$$
$$[cosh(0.5 s_1^\star H^\star) 0.5 s_1^\star H^\star - sinh(0.5 s_1^\star H^\star)]$$

$$b_1 = s_1^\star \xi_1^\star sinh(0.5 s_1^\star H^\star)$$
$$[cosh(0.5 s_2^\star H^\star) 0.5 s_2^\star H^\star - sinh(0.5 s_2^\star H^\star)]$$

$$a_2 = \xi_2^\star sinh(0.5 s_2^\star H^\star) cosh(0.5 s_1^\star H^\star)$$
$$b_2 = \xi_1^\star sinh(0.5 s_1^\star H^\star) cosh(0.5 s_2^\star H^\star)$$

$$s_1^\star = \left(\frac{\lambda_1 + \sqrt{\lambda_1^2 - 4\omega_1}}{2}\right)^{1/2},$$
$$s_2^\star = \left(\frac{\lambda_1 - \sqrt{\lambda_1^2 - 4\omega_1}}{2}\right)^{1/2}$$

$$\lambda_1^\star = \frac{N^2 + M^2(1-N^2)L^2}{L^2},$$
$$\omega_1^\star = \frac{N^2 M^2}{L^2} \quad ,$$

$$\xi_1^\star = \frac{M^2(1-N^2) - s_1^2,}{2N^2 s_1^2} \quad ,$$
$$\xi_2^\star = \frac{M^2(1-N^2) - s_2^2,}{2N^2 s_2^2} \quad ,$$

$$N = \left(\frac{\chi}{2\mu+\chi}\right)^{\frac{1}{2}}, L^\star = \frac{\left(\frac{\chi}{4\mu}\right)^{\frac{1}{2}}}{H_0} \quad ,$$
$$M = B_0 H_0 \left(\frac{\sigma}{\mu}\right)^{\frac{1}{2}}$$

Using the B.C, integrating the equation (16)

$$\frac{dp^\star}{dx} = 0 \ \text{ at } \ x^\star = 0$$

$$\frac{dp_i^\star}{dx} = \frac{-12x}{Q_i^\star(H_i^\star,N,L,M,\Psi,c^\star)} \qquad i = 1,2 \tag{18}$$

where
$p_1^\star$ denotes the pressure with step and $p_2^\star$ without step.

and
$H_i^\star = H_1^\star \quad for \quad 0 \le x \le K$
$= H_2^\star \quad for \quad K \le x \le 1$

The (B.C's) applicable for pressure are

$$p_1^\star = p_2^\star \quad at \quad x^\star = K$$
$$p_2^\star = 0 \quad at \quad x^\star = 1 \tag{19}$$

where K denotes the step size

Solution of equation (18) subject to pressure boundary condition (19), leads to the non dimensional pressure of the bearing considering the roughness effect is obtained in the form

$$E(p_1^\star) = 6\left[\frac{(K^2 - x^{\star 2})}{Q_1^\star(H_1^\star,N,L,M,\Psi,c^\star)} + \frac{(1-K^2)}{Q_2^\star(H_2^\star,N,L,M,\Psi,c^\star)}\right] \tag{20}$$

$$E(p_2^\star) = 6\left[\frac{(1-x^{\star 2})}{Q_2^\star(H_2^\star,N,L,M,\Psi,c^\star)}\right] \tag{21}$$

The expected work load $E(w)$ is obtained as

$$E(w) = 2b\int_0^{KL} E(p_1)dx + 2b\int_{KL}^{L} E(p_2)dx \tag{22}$$

The non-dimensionless expression of work load is given by

$$E(w^\star) = \left[\frac{K^3}{Q_1^\star(H_1^\star,N,L,M,\Psi,c^\star)} + \frac{(1-K^3)}{Q_2^\star(H_2^\star,N,L,M,\Psi,c^\star)}\right] \tag{23}$$

4. RESULTS AND DISCUSSIONS

Squeeze film lubrication between porous parallel stepped plates with micropolar fluid is studied in this paper. Two non-dimensional parameters, such as the coupling number N and length $L^\star$ that defines the interaction between fluid clearance, are used to describe the microplar fluid. The impact of the magnetic field $M$and the non-magnetic case is compared. Also, the surface roughness parameter c is analyzed with the presence of porosity in the bearing system.

4.1 Squeeze Film Pressure

A plot of pressure vs. distance for various values of coupling number N with $M = 5$, $L^\star = 0.15$, $K = 0.6$, $\Psi = 0.01$, $c = 0.3$ is shown in Figure-2. From the figure, it is observed that with increase in N coupling number the squeeze film pressure is also raising. A variation of pressure with distance is taken for distinct values of M

ARPN Journal of Engineering and Applied Sciences

with $N = 0.6$, $L^{\star} = 0.15$, $K = 0.6$, $\Psi = 0.01$, $c = 0.3$ as shown in Figure-3, and from the graph it is evident that pressure increases for increasing parameters of M. Figure.4 depicts the variation made for pressure verses distance for various c of roughness parameter with $N = 0.6$, $L^{\star} = 0.15$, $K = 0.6$, $M = 5$, $\Psi = 0.01$,. According to the graph it is evident that the pressure increases as c's value raises.

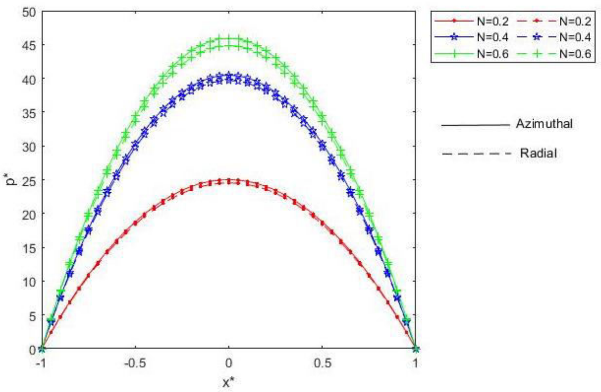

Figure-2. Non-dimensional pressure with distance for coupling number N.

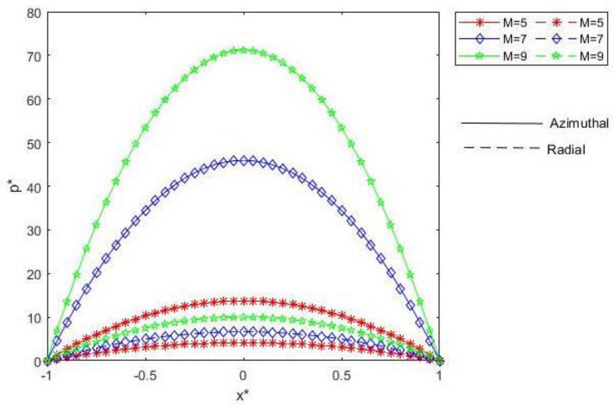

Figure-3. Plot of Pressure with distance for Hartmann number M.

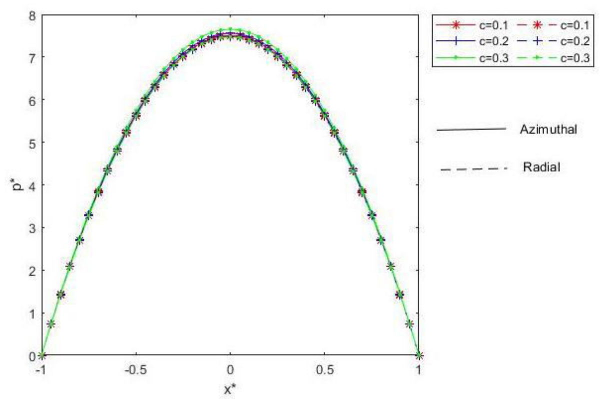

Figure-4. Plot of Pressure with distance for c.

4.2 Workload

A plot of workload versus height for distinct values of coupling number N with $M = 5$, $L^{\star} = 0.015$, $c = 0.3$, $K = 0.6$, $\Psi = 0.01$ is depicted in Figure-5. The figure shows that the workload increases with the coupling number N. A variation of workload with height for various values of Hartmann constant M when $L^{\star} = 0.015$, $K = 0.6$, $\Psi = 0.01$, $N = 0.6$, is taken in Figure-6. From the graph it is evident that the workload increases when the value of parameter M increases. Figure-7 depicts the variation of work load vs height for diverse values of c with $K = 0.6$, $M = 5$, $N = 0.6$, $\Psi = 0.01$. A comparison is made for magnetic and non-magnetic cases with different roughness parameters $c = 0.1,0.2,0.3$. For the same values of c the workload of the bearing for the magnetic case is more than the non magnetic case under the same situation. A variation of workload versus height for diverse values of K with $c = 0.3$, $M = 5$, $N = 0.6$, $\Psi = 0.01$ is depicted in Figure-8. From the graph it is noted that while increasing the step height K the workload decreases significantly. Plot of workload and height for diverse values of Ψ with $N = 0.6$, $M = 5$, $K = 0.6$, $c = 0.3$, $L^{\star} = 0.015$ is shown in figure.9, from which it is clear that the porosity of the material significantly decreases the workload of the bearing in comparison to the solid case.

VOL. 18, NO. 3, FEBRUARY 2023 ISSN 1819-6608
ARPN Journal of Engineering and Applied Sciences

www.arpnjournals.com

Table-1. Comparison of the workload for the case with MHD and without MHD for different values of roughness parameter c=0.1, 0.2, 0.3 with N=0.6, K=0.6. $L^{\star}$=0.015, Ψ=0.01.

	Magnetic case when Hartmann number (M=3)		
Roughness parameter	**c=0.1**	**c=0.2**	**c=0.3**
	6.277	6.3799	6.5626
	5.3641	5.435	5.56
Azimuthal	4.7685	4.8222	4.9167
	4.3637	4.4078	4.4853
	4.0785	4.1169	4.1844
	3.8709	3.9058	3.9672
	3.7156	3.7482	3.8057
	3.5963	3.6274	3.6823
	3.5025	3.5326	3.5857
	3.4271	3.4564	3.5083
	3.365	3.3938	3.4448
	6.2367	6.2159	6.1819
	5.3376	5.3269	5.3093
Radial	4.7489	4.7428	4.7326
	4.3479	4.3437	4.3367
	4.0648	4.0613	4.0555
	3.8585	3.8551	3.8495
	3.7038	3.7003	3.6945
	3.585	3.5812	3.575
	3.4914	3.4873	3.4807
	3.4161	3.4118	3.4047
	3.3541	3.3495	3.3421
	Non-magnetic case when Hartmann number (M=0)		
	c=0.1	c=0.2	c=0.3
	4.9763	5.0383	5.1471
	4.2329	4.2723	4.3412
	3.7063	3.7322	3.7771
Azimuthal	3.3254	3.3429	3.3731
	3.0444	3.0566	3.0774
	2.8334	2.842	2.8566
	2.6723	2.6785	2.689
	2.5474	2.5519	2.5597
	2.4492	2.4526	2.4584
	2.3712	2.3737	2.3781
	2.3084	2.3103	2.3137
	4.9457	4.9144	4.8637
	4.2132	4.1932	4.1605
	3.6933	3.6801	3.6585
	3.3167	3.3077	3.293
Radial	3.0384	3.0322	3.022
	2.8291	2.8247	2.8175
	2.6692	2.666	2.6608
	2.5451	2.5428	2.5389
	2.4475	2.4458	2.4429
	2.3699	2.3686	2.3664
	2.3074	2.3064	2.3047

Table-2. Variation of Workload verses height for different values of step height K with $M = 5$, $N = 0.6$, $c = 0.3$, $L^* = 0.015$, $\Psi = 0.01$.

Step height	Azimuthal	Radial
	19.7525	19.1559
	18.0218	17.562
	16.7012	16.3259
	15.6764	15.3538
	14.8659	14.5766
K=0.5	14.2119	13.9442
	13.6741	13.4206
	13.2236	12.9797
	12.84	12.6028
	12.5084	12.276
	12.2182	11.9892
	15.8279	15.3799
	14.1802	13.8625
	12.923	12.6857
	11.9474	11.7603
	11.1758	11.0205
K=0.7	10.5533	10.4184
	10.0412	9.9199
	9.6123	9.5002
	9.2471	9.1413
	8.9315	8.8302
	8.6552	8.5572
	12.7854	12.4526
	11.4562	11.2285
	10.4419	10.2792
	9.6549	9.5327
	9.0325	8.9358
K=0.8	8.5302	8.4501
	8.1171	8.0479
	7.7712	7.7093
	7.4765	7.4198
	7.2219	7.1689
	6.999	6.9486

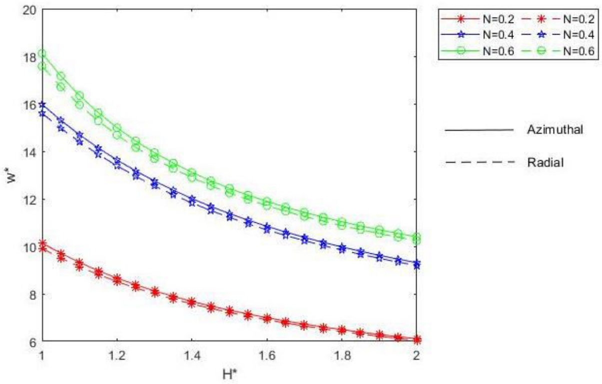

Figure-5. Non-dimensional work load with height for coupling number N.

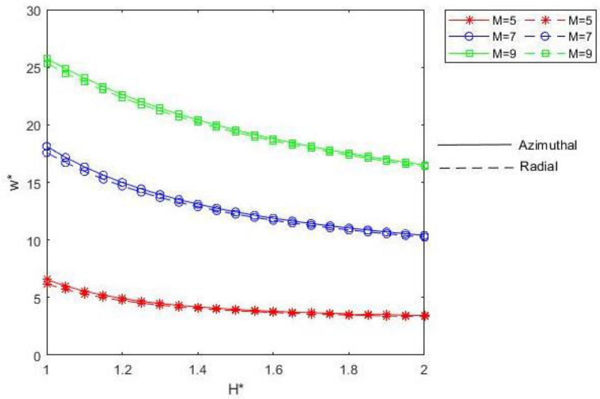

Figure-6. Variation of non-dimensional work load with height for Hartmann number M.

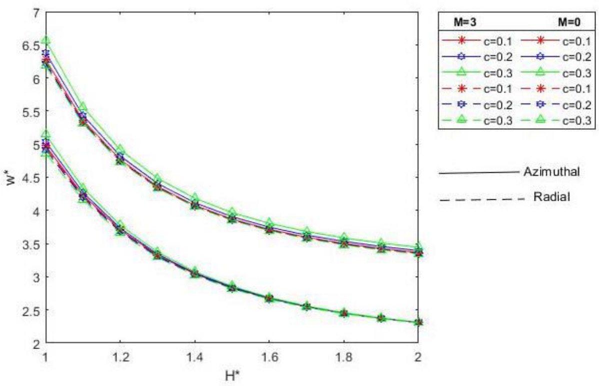

Figure-7. Plot of work load with height for c.

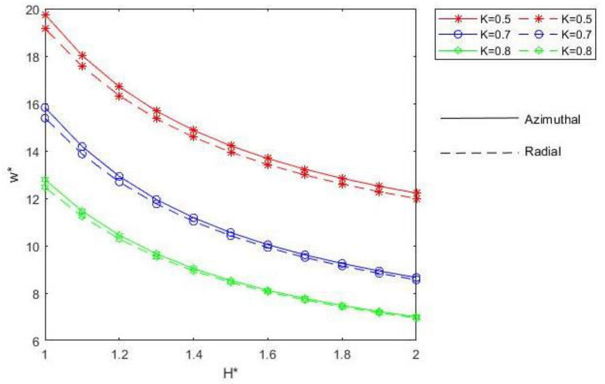

Figure-8. variation of work load with height for K.

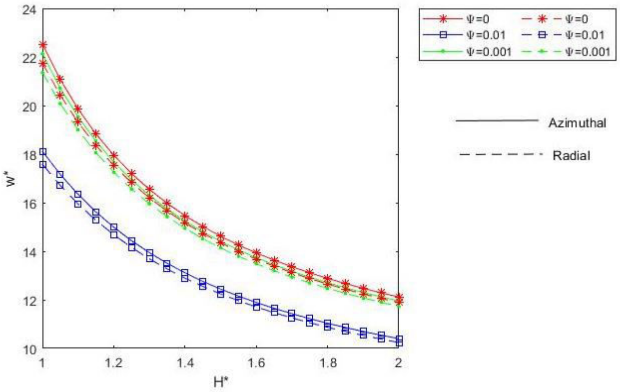

Figure-9. Non-dimensional work load with height for permeability parameter Ψ.

5. CONCLUSIONS

This paper forecasts the impact of micropolar fluid, applied magnetic field, and surface roughness on the squeeze film lubricating properties between porous parallel stepped plates using Eringen's micropolar fluid theory. The findings below are derived from the computed results.

a) The impact of micropolar increases the pressure and workload.

b) The performance of the bearing is affected by the bearing surface's porous facing as it decreases the workload.

c) The selection of lubricants with appropriate microstructure additives can minimize the adverse impact of the porous facing on the bearing surface.

d) Magnetic field enhances the performance of the bearing compared to non-magnetic field case.

e) Surface roughness increases the pressure and workload with increas in c.

REFERENCES

[1] Brinda Halambi, and B. N. Hanumagowda. 2018. Effect of hydromagnetic squeeze film lubrication of micropolar fluid between two elliptical plates. International Journal of Mechanical Engineering and Technology. 9(8): 939-947.

[2] N. M. Bujurke and R. B. Kudenatti. 2007. MHD Lubrication flow between rough rectangular plates. Fluid mechanics research. 39(4): 334-345.

[3] H. Christensen, K. C. Tonder. 1969. Tribology of rough surfaces: Parametric study and comparison of lubrication models. SINTEF Report No.22/69-18.

[4] A. C. Eringen. 1966. Theory of micropolar fluids. Journal of Mathematics and Mechanics. 16: 1-18.

[5] A. C. Eringen. 1964. Simple microfluids. Int. J. of Engg. Science. 2(2): 205-217.

[6] B. J. Hamrock. 1994. Fundamental of fluid film lubrication. New york, McGraw-Hill.

[7] B. N. Hanumagowda, A. Siddangouda, C. S. Nagarajappa, J. Santhosh Kumar. 2018. Hydromagnetic Squeeze Film Lubrication between Parallel Stepped Plates. In International Journal of Research in Engineering, IT and Social Sciences. Vol. 08.

[8] B. Halambi, B. N. Hanumagowda. 2021. Micropolar Squeeze Film Lubrication Analysis between Rough Porous Elliptical Plates and Surface Roughness Effects under the MHD. Ilkogretim Online-Elementary Education Online. 20(4): 307-319.

[9] B. N. Hanumagowda , N. Chaithra, H. S. Doreswamy, and A. Salma. 2020. Combined effect of surface roughness and micropolar fluids on squeeze film characteristics between rough flat plate and curved annular plates. Malaya Journal of Matematik. 8(2): 570-575.

[10] D. F. Hays. 1963. Squeeze films for rectangular plates. J. Fluids Eng. 85(2): 243-246.

[11] S. Kesavan, A. J. Chamkha and S. K. Narayanan. 2014. Magnetohydrodynamic (MHD) squeeze film characteristics between finite porous parallel rectangular plates with surface roughness. International Journal of Numerical Methods for Heat and Fluid Flow. 24(7): 1595-1609.

[12] D. C. Kuzma. 1964. Magnetohydrodynamic squeeze films. Journal of Basic Engineering, ASME. 86(3): 441-444.

[13] J. R. Lin. 2003. Magnetohydrodynamics squeze film characteristics for finite rectangular plates. Industrial Lubrication and Tribology. 55(2): 84-89.

[14] Murmu and Rao, "Influence of surface roughness and pressure-dependent viscosity on load carrying mechanism in micropolar fluid squeeze film lubrication between circular stepped plates. Jurnal Tribologi 25, pp.146-166 (2020).

[15] N. B. Naduvinamani and S. Santosh. 2011. Micropolar fluid squeeze film lubrication of finite porous journal bearing. Tribology International. 44(4): 409-416.

[16] N. B. Naduvinamani and S. Shridevi. 2018. Squeeze film lubrication between porous parallel plates with magneto-hydrodynamic-micropolar fluid. Journal of Nanofluids. 7(6): 1233-1239.

[17] A. Siddangouda. 2015. Squeezing Film Characteristics for Micropolar Fluid between Porous Parallel Stepped Plates. Tribology in Industry. 37(1).

[18] J. B. Shukla. 1995. Hydromagnetic theory of squeeze films. Journal of Basic Engineering, ASME. 87: 142-144.

[19] A. Siddangouda. 2012. Surface roughness effects in porous inclined stepped composite bearings lubricated with micropolar fluid. Lubrication Science. 24(8): 339-359.